Proceedings of the International Symposium on Engineering Lessons Learned from
the 2011 Great East Japan Earthquake, March 1-4, 2012, Tokyo, Japan

SOME FEATURES OF WATER PRESSURE CHANGE DURING THE 2011 TOHOKU EARTHQUAKE

Hiroyuki MATSUMOTO[1], Shusaku INOUE[2] and Tatsuo OHMACHI[3]

[1] Research Scientist, Japan Agency for Marine-Earth Science and Technology,
Kanagawa, Japan, hmatsumoto@jamstec.go.jp
[2] Research Engineer, Takenaka Research and Development Institute,
Chiba, Japan, inoue.shuusaku@takenaka.co.jp
[3] President, Japan Dam Engineering Center, Tokyo, Japan,
Professor Emeritus, Tokyo Institute of Technology,
ohmachi@jdec.or.jp

ABSTRACT: Water pressure change have been recorded during the 2011 Tohoku earthquake (Mw9.0) by two ocean-bottom pressure gauges of the JAMSTEC cabled observatory, and they have been interpreted by the acquired data analysis and the dynamic tsunami computation. As a result, the water pressure data have demonstrated that two kinds of water waves involved in the tsunami generation process; one is water waves preceding the tsunami having relatively short period, which is dominated by the ocean-bottom acceleration, and the other is long period wave well known as tsunami.

Key Words: The 2011 Tohoku earthquake, tsunami, ocean-bottom pressure gauge, hydro-dynamic pressure, hydro-static pressure.

INTRODUCTION

On 11 March 2011, at 05:46 UTC, i.e., 14:46 in local time (JST), a mega-thrust earthquake of the moment magnitude Mw 9.0 occurred off Tohoku district, the north-eastern Japan, causing a devastating tsunami that resulted in over 15,800 people's fatalities as well as over 3,300 people's missing as of 20 January 2012, particularly in the Tohoku district. The earthquake is referred to as the 2011 Tohoku earthquake hereafter for a reason of brevity. The Tohoku earthquake is a typical shallow dipping interplate earthquake between the subducting Pacific plate and the overlaying the North American plate, but the extent of the fault rupture area was much larger than that of our experience in the modern Japanese history. As a result, we could not anticipate such plural segments simultaneously fractured (e.g., Hayashi et al., 2011), causing a large mega-thrust earthquake along the Japan Trench in the Tohoku region.

The Japan Meteorological Agency (JMA) is responsible for tsunami warning issue, and the first tsunami warning was issued at 14:49 (Ozaki, 2011). In the mean time, the giant tsunami hit the coastal area in the Tohoku district, therefore many tide gauge stations were saturated by recording the highest level of 9.3 m and they were washed away at last. This is why tide gauges could not capture the tsunami waveforms completely, however, the offshore observatories such as the ocean-bottom

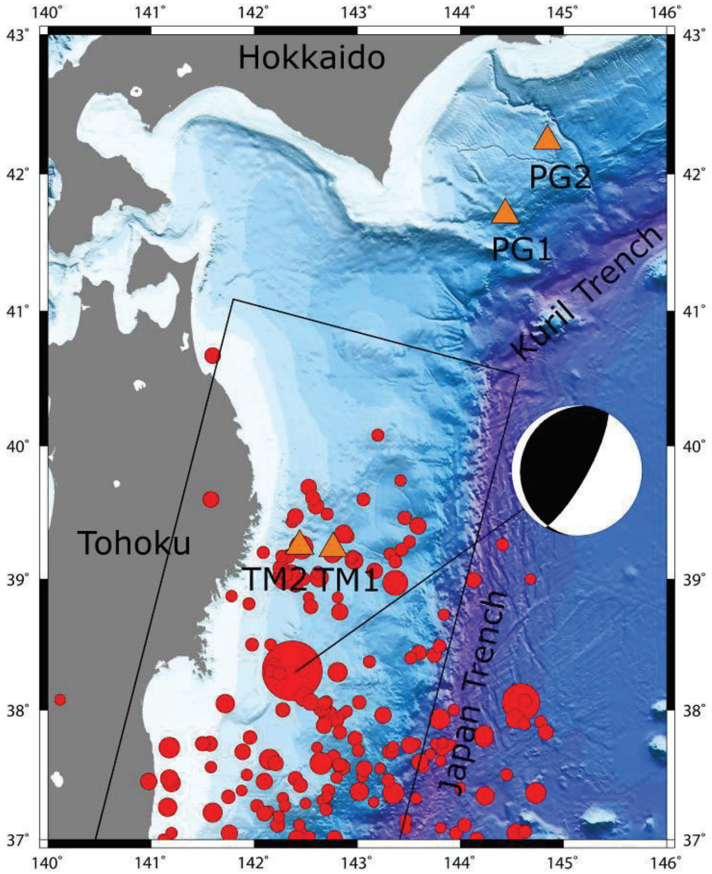

Fig. 1 Location map of the epicenter of the 2011 Tohoku earthquake, and the following aftershock distribution for a couple of days. Rectangular lines represent the fault plane's projection (USGS, 2011). Triangles represent the ocean-bottom pressure gauges, in which PGs and TMs are operated by JAMSTEC and University of Tokyo, respectively.

pressure gauges, the kinematic GPS buoys, and Deep-ocean Assessment and Reporting on Tsunami (DART) system except for their related landing facilities nearby were alive during the 2011 Tohoku earthquake, and they could fully capture the tsunami waveforms. It should be noted that JMA had raised, reduced or cancelled the tsunami warning grades by monitoring offshore tsunami waveforms in addition to the coastal tide gauges' recording (Ozaki, 2011). Thus, the offshore tsunami observatories have contributed to the tsunami warning in such a devastating tsunami being involved.

Japan Agency for Marine-Earth Science and Technology (JAMSTEC) is one of the institutions being operating some offshore cabled observatories in the seismogenic zone around Japan, and among which one observatory has been deployed off Hokkaido, the northern Japan since 1999 (Hirata et al., 2002). The JAMSTEC cabled observatory off Hokkaido consists of three ocean-bottom seismometers (OBSs) and two ocean-bottom pressure gauges (PGs), and their dataset are sent to the JAMSTEC in real-time (Fig. 1). Of course, the JAMSTEC cabled observatory was working well during the 2011 Tohoku earthquake, and it obtained all of the dataset.

In the present paper, at first we report the water pressure change recorded by the JAMSTEC's ocean-bottom pressure gauges and their interpretations by analyzing together with the ocean-bottom seismometers, because unrevealed features would be found in these invaluable records. We processed the original data from the raw frequency datasets regarding temperature and pressure, which made us possible to approach the higher frequency fluctuation than the tsunami. Finally we tried to reproduce the series of water pressure change from the 2011 Tohoku earthquake by means of tsunami computation taking into account the seismic fault rupture.

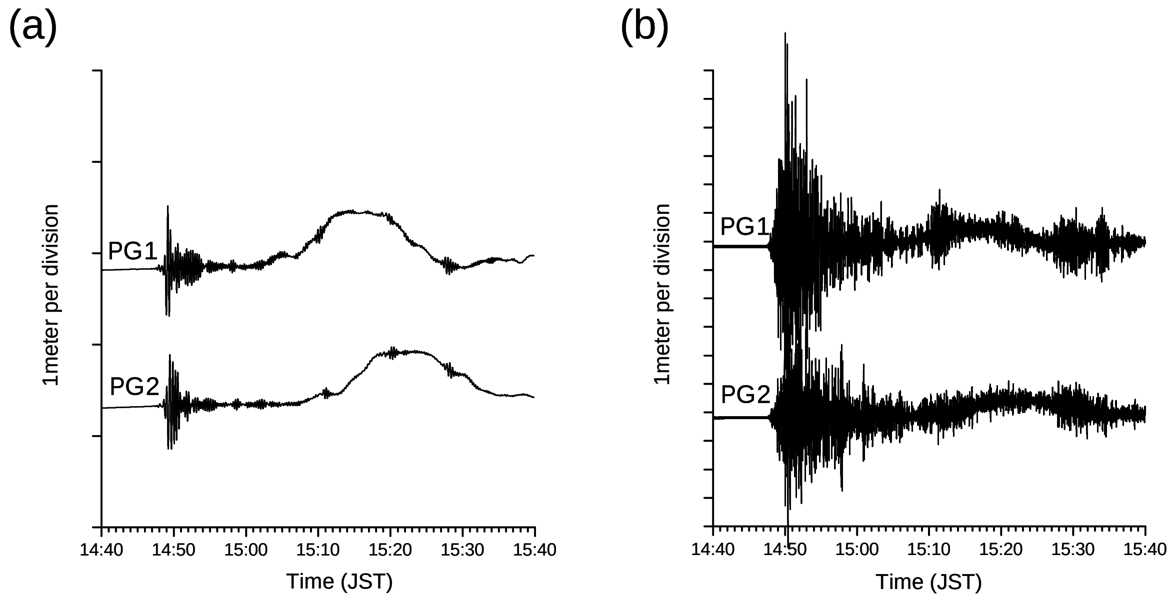

Fig. 2 Equivalent water height of water pressure recorded by the ocean-bottom pressure gauges during the 2011 Tohoku earthquake (a) after applying low-pass filtering and (b) their originals processed from the temperature and the pressure frequencies.

TSUNAMI DETECTED BY OCEAN-BOTTOM PRESSURE GAUGES

JAMSTEC's two ocean-bottom pressure gauges are located approximately 400 km north from the epicenter of the 2011 Tohoku earthquake (Fig. 1). The both ocean-bottom pressure gauges are deployed at a water depth of about 2,200 meters. Because the original water pressure waveforms during the earthquake contain the tide, the seismic wave, and the tsunami etc., either low-pass or band-pass filtering is usually applied to the originals in order to extract the tsunami signals. Figure 2(a) shows the observed water pressure waveforms during the 2011 Tohoku earthquake after applying the low-pass filtering of 100 s. The amplitude represents the equivalent water height of the hydro-static pressure. Although the low-pass filtering is applied to the originals, water pressure perturbations still left in the water pressure following the earthquake origin at 14:46. Tsunami signals can be identified by gradual rise followed by the highest crest. The first tsunami arrivals are at 15:02 and at 15:08 for PG1 and PG2, respectively. Small peaks are locally visible during the gradual rise before the highest crest at the both PGs. The maximum height of tsunami signals are about 0.7 m at 15:05 and at 15:11 for PG1 and PG2, respectively. Although the tsunami arrival times differ, its shapes are very similar each other.

By the way, the other ocean-bottom pressure gauges, TM1 and TM2 and the kinematic GPS buoy near the tsunami source, i.e., they are located at approximately 39 ^{o}N in latitude, recorded impulsive tsunami waveforms with its duration of about 5 min and height of 5 meters after the initial gradual rise, whereas the JAMSTEC's PGs did not record such unique waveforms. Needless to say, these waveforms have contributed to evaluate the seismic fault models based on the tsunami waveforms (e.g., Fujii et al., 2011; Maeda et al., 2011), and the tsunami source extent by means of their travel time (e.g., Hayashi et al. 2011). Thus, the offshore recorded tsunamis have been used not only in the tsunami warning issue but also in the tsunami studies after the 2011 Tohoku earthquake, however, the tsunami signals have been exclusively used in their studies.

Since the original recorded water pressure is usually contaminated by seismic waves as mentioned

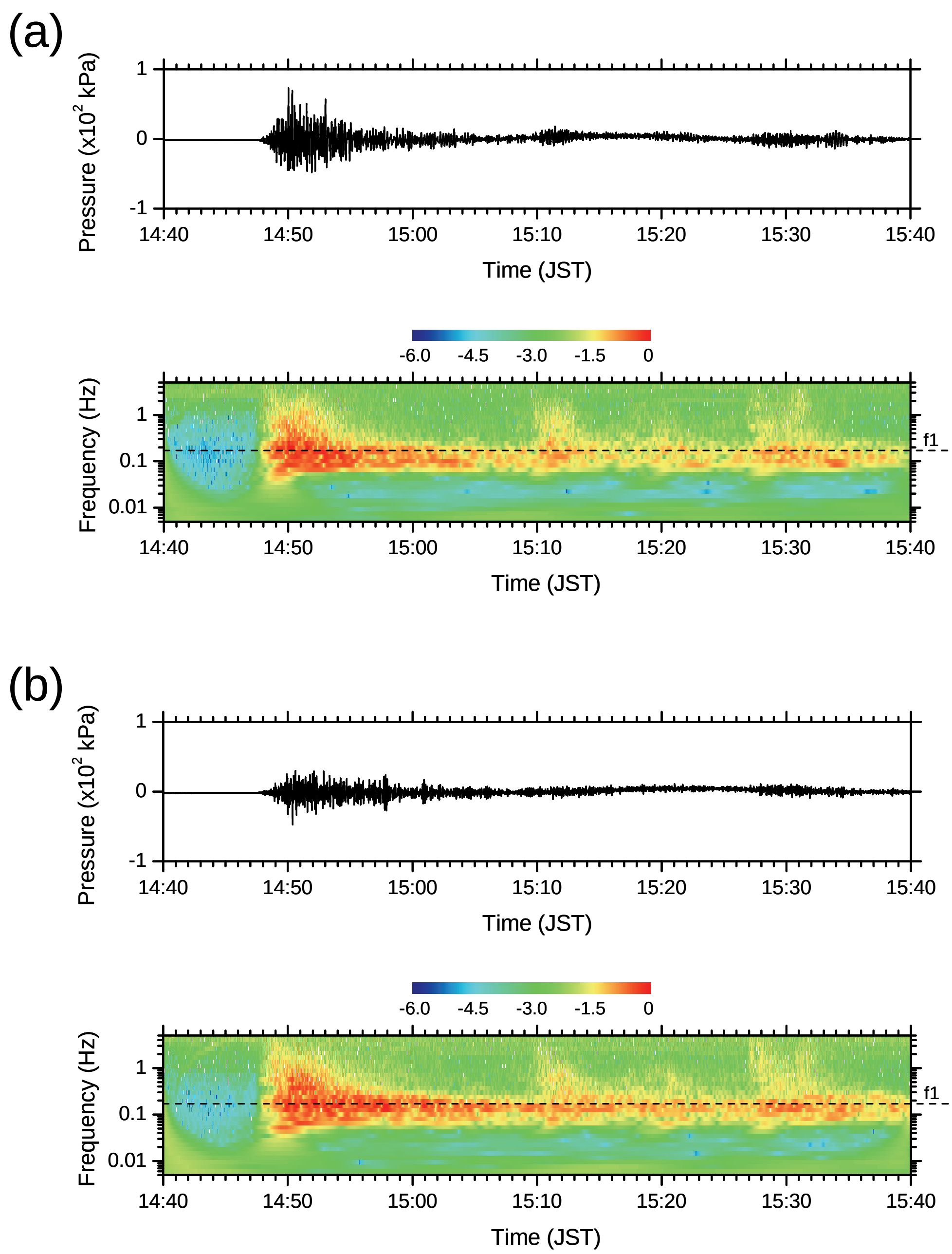

Fig. 3 Spectrograms of water pressure and the original waveforms of (a) PG1 and (b) PG2, in which f1 indicates the characterized frequency of a fundamental resonant mode of water layer.

above, we process the whole data in the following section. The whole water pressure waveforms should be explained in the viewpoint of technical development on real-time tsunami detection.

WATER PRESSURE CHANGE ANALYSIS

PGs measure high frequency quartz oscillations, and then they are converted to the physical value of water pressure with compensating by thermal effect. The higher water pressure data is sampled, the lower the resolution results in this kind of pressure gauge. As for the JAMSTEC's PGs, 1 Hz sampled data is usually processed, but 10 Hz sampled dataset could be reproduced in the present case

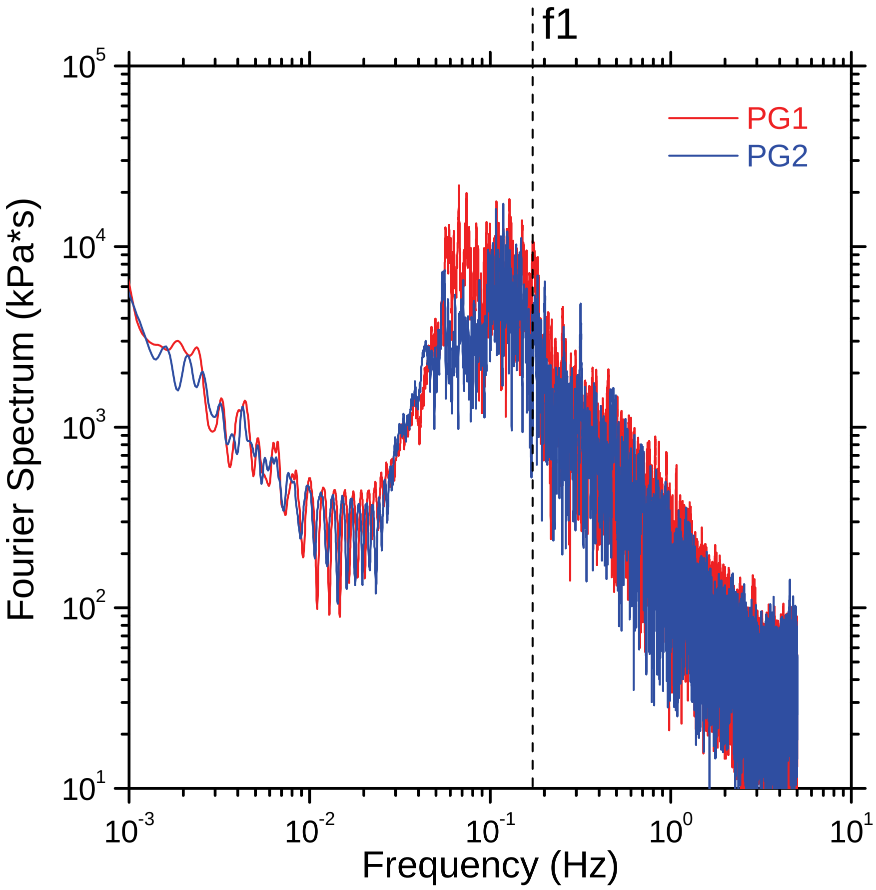

Fig. 4 Fourier spectrum of PG1 and PG2 in which vertical dashed line denoted by f1 indicates the characterized frequency of a fundamental acoustic resonant mode of water layer.

because S/N ratio was relatively better during the 2011 Tohoku earthquake than other usual events. Thermal correction on physical water pressure is carried out by considering its change as time series. After thus processing the original frequencies compensating the thermal effect, we could obtain the 10 Hz sampled water pressure waveforms during the 2011 Tohoku earthquake (Fig. 2(b)).

We have analyzed the obtained PGs dataset by depicting spectrograms. Numerical technique to analyze 10 Hz sampled PGs dataset is as follows;

1) 1 hour data of pressure gauge including the 2011 Tohoku earthquake is collected. In the current analysis, the start time is set to be 14:40:00 JST.

2) We divide the frequency from 0.003 Hz to 5 Hz into 33 sections as formed exponentially, i.e., linearly in logarithmic scale.

3) Band-pass filtering of each section above is applied to the entire 1 hour dataset.

4) Envelopes of the band-pass filtered waveforms for each section are aligned to get absolute amplitude, and spectrogram of PGs data during the 2011 Tohoku earthquake can be made.

5) But amplitude normalized by the maximal value is depicted in the logarithmic scale so that the predominant frequencies would be emphasized in the present paper.

After applying the procedure above, we could obtain the spectrograms as shown in Fig. 3, in which f1 indicates the characterized frequency of a fundamental acoustic resonant mode of water layer assuming the rigid ocean-bottom expressed as,

$$f1 = c/4H \tag{1}$$

where H and c are water depth and sound velocity, respectively. Lasting signals having slight lower frequency than f1 appears for a long-time, whereas high frequency signals were decayed immediately after the earthquake. Aftershocks which occurred several times after the main shock emphasize higher frequency band. The tsunami signals could be recognized after 15:00 and 15:10 for PG1 and PG2, respectively, despite the intensity is rather small.

Focusing on the initial stage prior to the tsunami arrivals, Fourier spectra of PGs for the initial 10 min from the earthquake origin are made in Fig. 4. According to Fourier spectrum, the highest peaks of the both PGs are 0.05 to 0.1 Hz, which does not correspond to the characterized frequency of a fundamental acoustic resonant mode. Thus, an acoustic resonance was not excited at the location of JAMSTEC's PGs, because PGs were out of the tsunami source. The lower the frequency becomes, the larger the amplitude responses proportionally, which is attributed to the long-period tsunami component.

By the way, lasting signals recorded by PGs were dominated by acoustic resonances in the case of the 2003 Tokachi-oki earthquake of Mw8.3, which took place beneath the JAMSTEC cabled observatory (Nosov and Kolesov., 2007). Although both the 2003 Tokachi-oki earthquake and the 2011 Tohoku earthquake are tsunamigenic earthquakes, difference between two earthquakes is the near-field and intermediate-field events from the PGs' location. In the 2003 Tokachi-oki earthquake, acoustic resonances associate with the crustal movement was extremely excited in the tsunami source. In the case of 2011 Tohoku earthquake, however, such acoustic resonances were not remarkably recorded in the JAMSTEC's PGs data.

DISCUSSIONS

Implication of ocean-bottom seismometer

Our recent paper regarding the 2003 Tokachi-oki earthquake provides a cue to interpret the pressure waveforms recorded by the ocean-bottom pressure gauges (Bolshakova et al., 2011). We have introduced the characterized frequency of the fundamental acoustic resonant mode of water layer in the previous section. An additional characterized frequency should be notified, which is related to gravitational waves,

$$fg = (g/H)^{1/2} \tag{2}$$

where g is the acceleration due to the gravity. In the conditions of the planet earth, at any point of the world ocean, the characteristic frequency fg is always smaller than that of the fundamental acoustic resonant mode as same formula as Eq. (1),

$$f1 = c/4H \tag{3}$$

Frequencies fg and f1 divide into three frequency bands; "gravitational waves", "forced oscillations" and "hydro-acoustic waves". Generally, bottom oscillations of any frequency give rise to forced oscillations of water layer in the vicinity of tsunami source. Bottom oscillations of low-frequency ($f < fg$), additionally to the forced oscillations, generate gravitational waves which are radiated from the source. Bottom oscillations of high-frequency ($f1 < f$), additionally to the forced oscillations, produce hydro-acoustic waves. In the case of bottom oscillations of intermediate-frequency ($fg < f < f1$), the forced oscillations are extremely produced, whereas gravitational wave is not remarkable as well as acoustic resonances cannot be produced in the source.

Within the frequency band "forced oscillations", according to the Newton's second law, the following relation between the vertical component of bottom acceleration and variations of bottom pressure p must be fulfilled,

$$p = \rho H \alpha \tag{4}$$

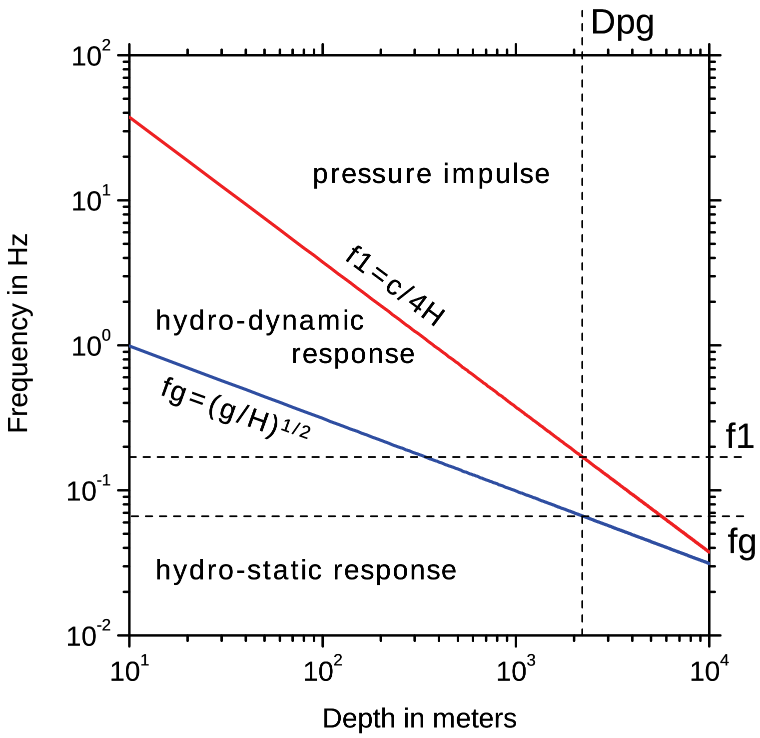

Fig. 5 Hydro-pressure responses related by the frequency vs. the water depth (reproduced from Bolshakova et al., 2011). Vertical dashed line denoted by Dpg indicates the water depth at which the ocean-bottom pressure gauges are deployed. Horizontal dashed lines denoted by f1 and fg indicate the characterized frequencies dividing frequency bands depending on the water depth..

where ρ and α are the density of water and the bottom acceleration, respectively. Hence, within the frequency band fg < f < f1, if the ocean-bottom pressure gauges and ocean-bottom seismometers are located close to each other, spectra of the bottom pressure and the bottom acceleration represented in pressure units with use of Eq. (4) are expected to coincide.

Within the frequency band “hydro-acoustic waves”, on the other hand, the bottom pressure forcing an abrupt bottom change is linked by the vertical component of bottom velocity by means of the Joukowsi’s formula,

$$p = \rho c u \tag{5}$$

where c and u are the acoustic velocity in water, i.e., approximately 1,500 m/s and the bottom rapid velocity, respectively.

In view of the theoretical bottom pressure formulas of these three frequency bands, i.e., because pressure of “gravitational waves” is isolated from the bottom frequency, and that of “forced oscillations” and “hydro-acoustic waves” are proportioned by “bottom acceleration” and “bottom velocity”, respectively, we can name these three frequency bands, “hydro-static response”, “hydro-dynamic response”, and “pressure impulse” for the frequency band of f < fg, fg < f < f1, and f1 < f, respectively (Fig. 5).

Ocean-bottom seismometers measure three components’ accelerations, whose orientations depend on the cable laying condition, therefore we correct them to the Gaussian coordinate, i.e., NS, EW, and UD components. We use converted water pressure by means of Eq. (4) of UD component of OBS1 and OBS3 which are located a few kilometers away from PG1 and PG2, respectively. The Fourier spectra compare each other in Fig. 6. A couple of vertical dashed lines stand for the appropriate positions of characterized frequencies of fg and f1. The Fourier spectra of the bottom pressure

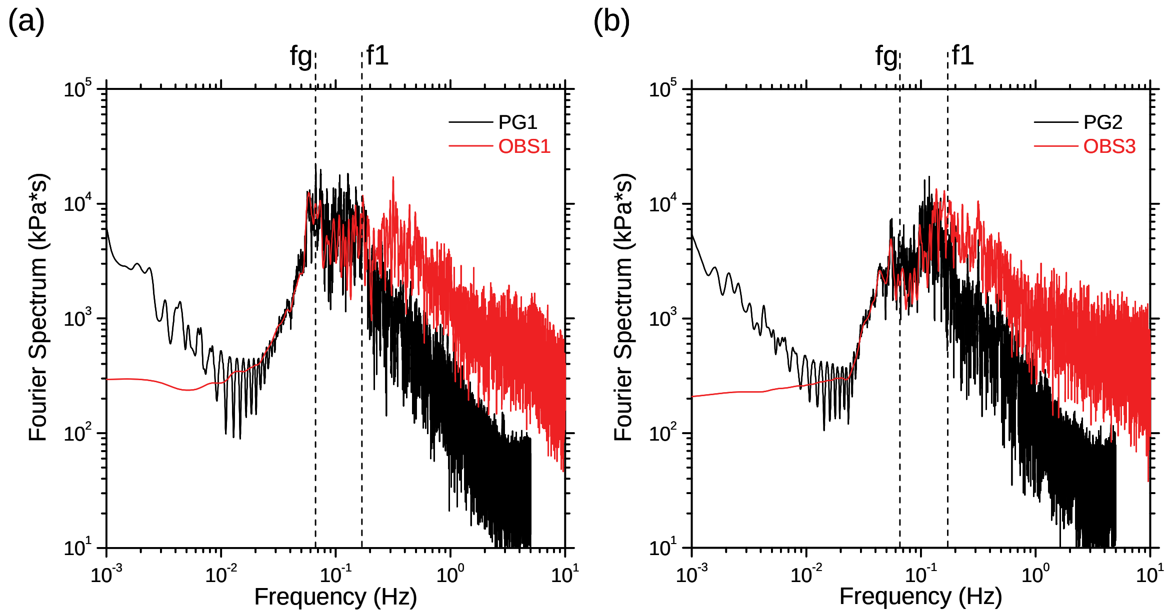

Fig. 6 Comparison of the Fourier spectra between the ocean-bottom pressure gauges and the ocean-bottom seismometer, i.e., acceleration nearby converted to water pressure during the 2011 Tohoku earthquake for (a) PG1 and (b) PG2. Vertical dashed lines denoted by fg and f1 indicate the characterized frequencies dividing hydro-dynamic and static pressure responses and the pressure impulse respectively.

roughly exhibit broadband peak between the frequencies of fg and f1. Similarly the Fourier spectra of UD acceleration depicted in Fig.6, and the peaks coincide to the frequency band between the characterized frequencies of fg and f1. Because the minimal frequency of the ocean-bottom seismometers' measurement is 0.05 Hz, the amplitude drops in the low-frequency. The most striking fact here consist in nearly ideal coincidence of the spectra of the bottom pressure and the bottom acceleration represented in pressure units with use of Eq. (4) within the frequency band "hydro-dynamic response" between the characterized frequencies of fg and f1. The bottom pressures seemingly follow the bottom accelerations in this frequency band. Note that outside of the higher frequency band, i.e., "pressure impulse", the spectra turn out to be essentially different. This means that the most part of the observed water pressure by PGs are predominated by not the acoustic waves but the bottom acceleration. The moderate-to-long peak frequency implies that the Rayleigh wave may contribute to induce the bottom pressure change. Filloux (1982) reported that the bottom pressure change is attributed to the accelerations in the far-field based on his field observations. Thus, this is not a new empirical result, but this is the first comparison between the ocean-bottom pressure and the ocean-bottom acceleration during such a large tsunamigenic earthquake in the intermediate-field.

Implementation of tsunami computation

We reproduce the water pressure from the 2011 Tohoku earthquake to verify our data processing of the ocean-bottom pressure gauges, and how the tsunami radiates from the tsunami source along the Japan-Kuril Trench system by means of tsunami computation.

A seismic faulting causing water mass movement is assumed from the seismic fault model by USGS (2011), that is based on the teleseismic broadband P-waves, the broadband SH-waves, and long period surface waves. The fault geometry is as follows. The size of the fault plane is 625 km along the strike and 260 km along the dip, in which 325 sub-faults are consisted. The depths of sub-faults vary from 7.5 km to 50.1 km, and the strike and dip angles are uniformly 194.4 ^{o} and 10.2 ^{o},

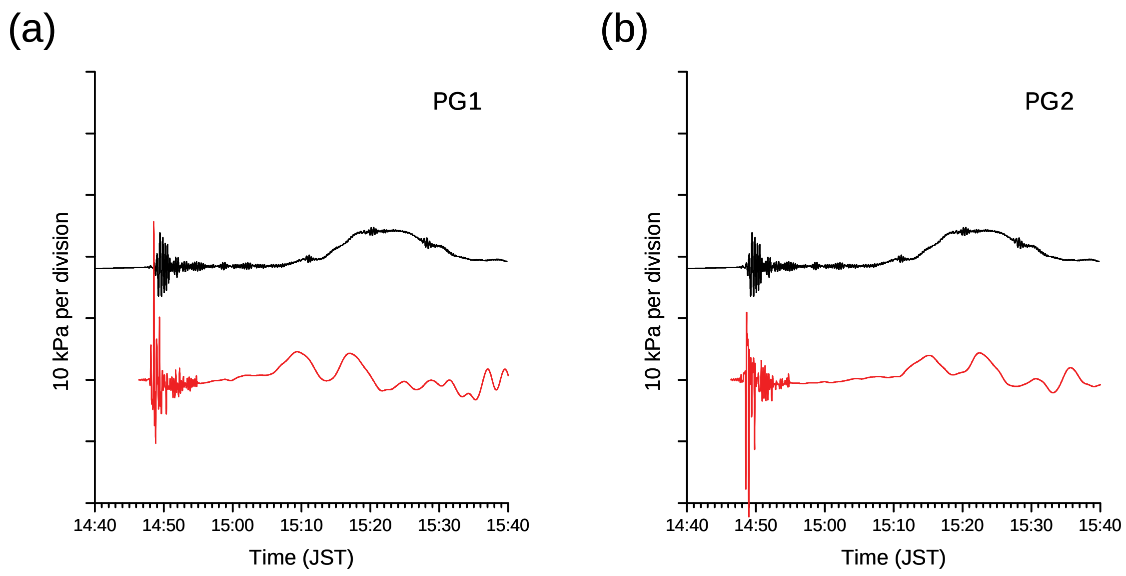

Fig. 7 Comparison of the computed water pressure change (red line) from the 2011 Tohoku earthquake in terms of the seismic fault model by USGS (2011) with the observed one (black line) for (a) PG1 and (b) PG2.

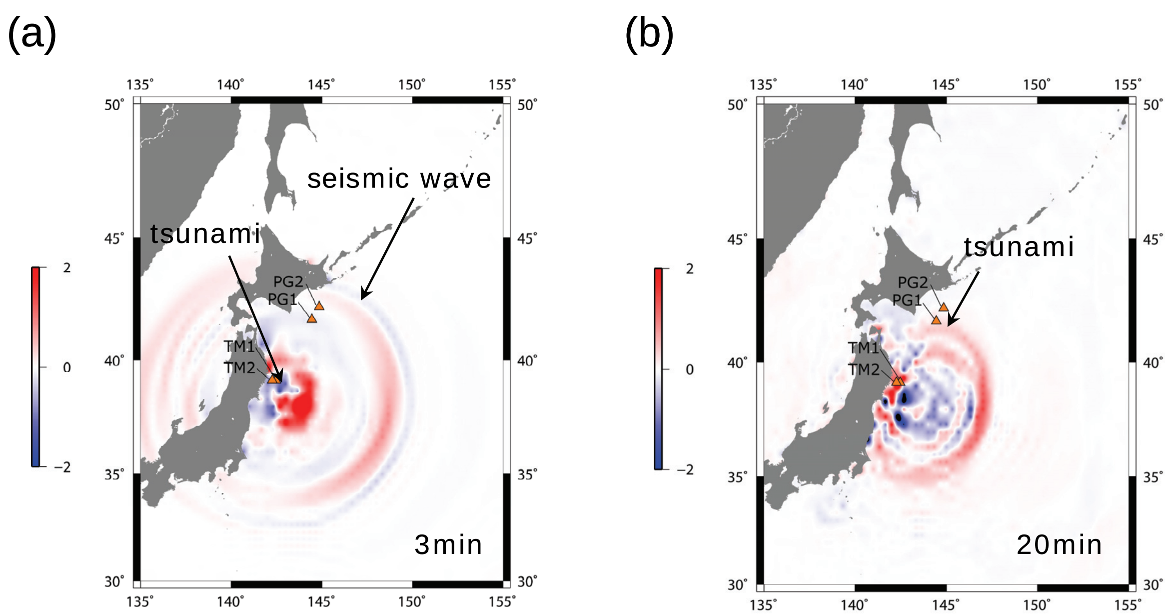

Fig. 8 Snapshots of (a) the tsunami generation, and followed by (b) the propagation. Time inset the figure represents the elapsed time from the earthquake origin. Scale bar stands for water level in meters.

respectively for the entire sub-faults. Slip, rake, and rupture start time are given to each sub-fault, and the total duration time of the fault rupture results in about 230 s. Details of the present tsunami computation technique are described in Ohmachi et al. (2001). We first calculate seismic waves with its frequency band up to 0.125 Hz, and then it is used as boundary conditions for tsunami generation. Thus, both the dynamic motion of the ocean-bottom and the rupture effect of seismic faulting are taken into account in a weak-coupled 3D fluid system, in the present tsunami computation. The computational domain extends from 30.00 ^{o}N to 50.00 ^{o}N in latitude and from 135.00 ^{o}E to 155.00 ^{o}E in longitude. Uniform 2 min in arc gridded bathymetric dataset made from GEBCO (British Oceanographic Data Centre, 1997) and 1,000 m grid in depth direction, and time step of 0.5 s are used in our tsunami computation. This means the total number of grid point result in more than 3.2 millions. Since the present tsunami computation is set to be very large, shallow water area is modeled too rough to reproduce the tsunami heights.

The computed water pressure changes are compared to the observed water pressure change of PGs in Fig. 7. Note that the observed water pressure is what after low-pass filtering as same as shown in Fig. 2(a), because the present computation on the seismic wave is carried out up to 0.125 Hz. Immediately after the earthquake, water pressure fluctuations are reproduced by seismic waves. Their amplitude and the duration time, and decay of the seismic effect coincide with each other qualitatively. The arrivals of the first tsunami of our computation are somewhat earlier than that of the observations. And the first arrival tsunamis exhibit very long period single waves in the observation, but two small peaks on the first tsunami are computed at both PGs. Nevertheless, the amplitudes of the first tsunami are fit to the observations. We use the slip distribution based on the seismic waves in the present tsunami computation. This is why relatively high-frequency phases might tend to be reproduced in our tsunami computation. The importance is that two kinds of water pressure change are reproduced from the seismic faulting.

Snapshots of the sea surface response at 3 min, and 20 min are displayed in Fig. 8. Seismic waves are radiated from the each sub-fault at 3 min, when the fault rupture is still going on. At that time, the tsunami caused by the static deformation is produced off Tohoku region along the Japan Trench. At 20 min, the tsunami is radiated to PGs. In general, tsunami energy is relatively large toward the normal of the fault strike direction. In the case of the 2011 Tohoku earthquake, the tsunami energy spreads toward the Tohoku region, since the fault strike is parallel to the Japan Trench. Our tsunami computation qualitatively demonstrates this phenomenon. According to the tsunami propagation (Fig. 8(b)), the first tsunami has two peaks before its arrival at PGs. Discrepancy of the first tsunami shape between the computations and the observations are attributed to the seismic models, e.g., asperity's distribution.

CONCLUSIONS

Water pressure change have been recorded during the 2011 Tohoku earthquake (Mw9.0) by two ocean-bottom pressure gauges of the JAMSTEC cabled observatory off Hokkaido, and they have been interpreted in terms of the data processing. The acquired data have demonstrated that two kinds of water waves involved in the tsunami generation process from the 2011 Tohoku earthquake; that is, one is water waves preceding the tsunami having relatively short period to the tsunami and the other is long period wave well known as tsunami. Their features are summarized as,

1. As for the tsunami, it was detected 16 min and 22 min after the main shock by two ocean-bottom pressure gauges located approximately 400 km north from the earthquake epicenter. The first tsunami had a maximum height of 0.7 m and its period of about 40 min. There is no significant difference except for the arrival time among two ocean-bottom pressure gauges. The tsunami had a gentle rise followed by a solitary wave with a height of about 3 m and duration of about 5min in the other similar ocean-bottom pressure gauges deployed near the tsunami source (e.g., Maeda et al., 2011), whereas such a solitary wave was not recorded by the JAMSTEC's ocean-bottom pressure gauges. This unique feature might be attributed to the tectonic mechanism. Difference of the tsunami features between two observatories are attributed not only to the source distance but also the directivity of the tsunami energy, because the JAMSTEC cabled observatory was located parallel to the seismic fault strike direction.

2. The water waves preceding the tsunami were detected in an early stage of the water pressure change. Comparing water pressure together with the data of the ocean-bottom seismometers nearby, it has been revealed that this is associated with the forced oscillation response of water layer by the bottom acceleration, i.e., hydro-dynamic response. This kind of waves was seemingly attributed to a moderate-to-large ocean-bottom displacement associated with the Rayleigh waves, because some

features similar to the seismic ocean-bottom displacement induced by the Rayleigh waves such as the directivity, an elliptical particle orbit, and a rather long predominant period. In addition, the preceding waves were also observed at several DART stations deployed in the Pacific Ocean (e.g., Hayashi et al., 2011). The pressure perturbations lasted much longer and had amplitude more than ten times larger than that associated with the tsunami, i.e., hydro-static response.

Although some unsolved problems, e.g., on the discrepancies of the tsunami arrival time or the first tsunami shape still remain, these two kinds of water waves could be reproduced by our dynamic 3D tsunami computation based on the seismic faulting process. Thus, the above-mentioned two kinds of water waves must be generated in the 2011 Tohoku earthquake.

ACKNOWLEDGMENTS

Fruitful discussions with Mikhail Nosov and Sergey Kolesov, M. V. Lomonosov Moscow State University were helpful to the present study. The ocean-bottom pressure gauges' and ocean-bottom seismometers' dataset were provided by JAMSTEC. The authors would like to thank those staffs who daily maintain the JAMSTEC cabled observatory. This study was partly supported by the Japan Society for the Promotion of Science (JSPS project 100423) and the Russian Foundation for Basic Research (RFBR project 10-05-92102) under the Japan-Russia Research Cooperative Program, and also the Grants-in-Aid for Scientific Research (Young scientist (C) 22710175) by JSPS.

REFERENCES

Bolshakova, A., Inoue, S., Kolesov, S., Matsumoto, H., Nosov, M. and Ohmachi, T. (2011). "Hydroacoustic effects in the 2003 Tokachi-oki tsunami source." *Russ. J. Earth. Sci.*, Vol. 12, ES2005, doi:10.2205/2011ES000509.

British Oceanographic Data Centre. (1997). "The centerary edition of the GEBCO digital atlas (CD-ROM)."

Filloux, J. H. (1982). "Tsunami record on the open ocean floor." *Geophys. Res. Lett.*, Vol. 9, 25-28.

Fujii, Y., Satake, K., Sakai, S., Shinohara, M. and Kanazawa, T. (2011). "Tsunami source of the 2011 off the pacific coast of Tohoku Earthquake." *Earth Plants Space*, Vol. 63, 815-820.

Hayashi, Y., Tsushima, H., Hirata, K., Kimura, K. And Maeda, K. (2011). "Tsunami source area of the 2011 off the Pacific coast of Tohoku Earthquake determined from tsunami arrival times at offshore observation stations." *Earth Plants Space*, Vol. 63, 809-813.

Hirata, K., Aoyagi, M., Mikada, H., Kawaguchi, K., Kaiho, Y., Iwase, R., Morita, S., Fujisawa, I., Sugioka, H., Mitsuzawa, K., Suyehiro, K., Kinoshita, H. and Fujiwara, N. (2002). "Real-time geophysical measurements on the deep seafloor using submarine cable in the southern Kurile subduction zone." *IEEE J. Ocean. Eng.*, Vol. 27, 170-181.

Maeda, T., Furumura, T., Sakai, S. And Shinohara, M. (2011). "Significant tsunami observed at ocean-bottom pressure gauges during the 2011 off the Pacific coast of Tohoku Earthquake." *Earth Plants Space*, Vol. 63, 803-808.

Nosov, M. and Kolesov, S. (2007). "Elastic oscillations of water column in the 2003 Tokachi-oki tsunami source: in-situ measurements and 3-D numerical modeling." *Nat. Haz. Earth Sys. Sci.*, Vol. 7, 243-249.

Ohmachi, T., Tsukiyama, H. and Matsumoto, H. (2001). "Simulation of tsunami induced by dynamic displacement of seabed due to seismic faulting." *Bull. Seism. Soc. Am.*, Vol. 91, 1898-1909.

Ozaki, T. (2011). "Outline of the 2011 off the Pacific coast of Tohoku Earthquake (Mw 9.0) -Tsunami warnings/advisories and observations-." *Earth Plants Space*, Vol. 63, 827-830.

U. S. Geological Survey. (2011). "Finite fault model, Updated result of the Mar 11, 2011 Mw9.0 earthquake offshore Honshu, Japan." http://earthquake.usgs.gov/earthquakes/eqinthenews/2011/usc0001xgp/finite_fault.php, accessed on 27 December 2011.